Evaluation of Well-defined Tool Surface Designs for Groundwood Pulping

Magnus Heldin * and Urban Wiklund

Groundwood pulping is a process in which logs are pressed against a rotating grinding stone. A conventional grinding stone is generally made of grinding particles in a vitrified matrix. As the particles are practically round, their contact with the wood is limited to occasional point contacts. The interaction between the particles and the wood occurs at random positions and at random times, only intermittently contributing to the defibration process. In this work, well-defined grinding tools with asperities giving line contacts rather than point contacts were tested. The tool surface asperities were elongated in shape and positioned with different density over the surface. The tools were tested in a lab-scale equipment at elevated temperatures, and their performance was compared to that of a conventional grinding stone. The grinding mechanisms varied between the different tools, and the specific grinding energy was reduced compared to the conventional tool.

Keywords: Groundwood pulping; Diamond tools; Energy consumption; Tomography; Grinding mechanisms

Contact information: Ångström Tribomaterials Group, Division of Applied Materials Science, Department of Engineering Sciences, Uppsala University, Box 534, 75121 Uppsala, Sweden;
** Corresponding author: magnus.heldin@angstrom.uu.se*

INTRODUCTION

Groundwood pulping is a mechanical pulping process in which wood logs are pressed against a rotating grinding stone to separate the fibers, creating pulp. The energy consumption is high in these processes, and most of the energy is lost through undesired viscoelastic deformation of the wood; only a minor part of the energy is beneficial to the separation of the fibers (Campbell 1934; Uhmeier and Salmén 1996). During grinding, the groundwood pulping processes produce pulp of all different fractions, from long slender fibers to fines. Controlling the characteristics of the pulp is desirable when making pulp to be used in different applications, as the requirements will differ. For instance, the fibers preferred when producing characteristics used in newsprint paper are not that suitable for reinforcement in polymers.

The process parameters have a strong influence on both the process itself and the properties of the produced pulp. The temperature at which the grinding takes place is probably the most well-known and most studied parameter. Softening of the wood will occur as the temperature is increased and, in the range of temperatures used in pulping processes, the softening hemicelluloses and lignin will affect the mechanical properties of the wood (Koran 1981; Blechschmidt *et al.* 1986) and facilitate defibration.

Other influential parameters are the properties of the tool. Conventional grinding stones consist of grinding particles fixed in a matrix, typically alumina particles in a vitrified matrix. The particles are randomly distributed over the surface of these grinding

stones, making the occasional contacts between grinding particles and wood fibers very stochastic in nature.

The size and shape of the particles are important in the defibration process, affecting the mechanisms in the contact between the grinding stone and the wood, and changing the energy consumption of the process as well as the quality of the fibers produced (Enström *et al.* 1990; Sandås and Lönnberg 1990; Sandås 1991a,b; Lönnberg *et al.* 1996; Tuovinen *et al.* 2008). Fatigue is believed to be an important part of the defibration (Salmi *et al.* 2012a,b) and by profiling the grinding stone, *i.e.*, creating a sinusoidal topography along the circumference of the stone, fatigue can be enhanced in the wood during grinding, while also reducing the energy consumption (Björkqvist and Lucander 2001; Björkqvist *et al.* 2007). The surface pattern can be used to influence the character of the released fibers. Tools with a serrated profile across the width of a conventional grinding stone have been shown to increase the fraction of fines in the pulp (Nurminen *et al*. 2018).

The distribution of particles in the grinding stone surface can be changed from random, as in conventional stones, to controlled (Tuovinen *et al.* 2009; Tuovinen and Fardim 2015) allowing greater control of the particle interactions with the wood during grinding.

Most previous research on wood grinding has employed grinding tools where, in some form, particles are fixed in a supportive matrix. This has generally meant that the particles are round in shape and their interactions with the wood are in the form of point contacts. However, extremely well-defined grinding surfaces have been produced using diamond deposition on patterned silicon and have been used to grind other types of materials (Gåhlin *et al.* 1999). The same production technique has been used to create embossing tools with surfaces upon which the asperities had an elongated profile (Pettersson and Jacobson 2006). In this work, grinding surfaces with surface asperities designed to give line contacts, instead of point contacts, were produced. The use of such tool surfaces has the potential of not only affecting the energy consumption in pulp production, but also the fibrillation and transport of fibers out of the grinding zone. This means that the tools can be tailored to produce fibers with different characteristics.

This work investigated the influence of three different well-defined grinding surfaces on mechanisms and energy consumption during grinding at different temperatures in a lab-scale grinding setup. A piece of a conventional grinding stone was used for comparison.

EXPERIMENTAL

The equipment and method used in this work are described in greater detail in a previous work (Heldin and Wiklund 2019) and will only briefly be described here.

Grinding Experiments

A setup similar to a lathe was used for the grinding experiments. Flat patterned grinding tools were pressed against a rotating cylindrical wood specimen by a spring-loaded tool holder, instrumented to measure the normal and tangential forces affecting the tool. The setup was placed inside a pressure chamber to allow for a test environment similar to the industrial grinding process, which is carried out at elevated pressure using

steam. The test parameters used are displayed in Table 1. After each test the released fibers were collected for analysis.

The well-defined grinding tools used were all 5 × 5 mm^2 and made of nanocrystalline diamond films soldered to steel backings. One tool surface consisted of long parallel ridges (S_{Long}) that were 89 µm in base width, 64 µm high, and spanning the full width of the tool, as shown in Figs. 1a and b. A second tool surface with a sparse pattern of shorter ridges (S_{Sparse}) had 500 µm long, 86 µm wide, and 61 µm high ridges distributed over its surface (see Figs. 1c and d). The third tool surface, with a dense pattern of short ridges (S_{Dense}), had 260 µm long, 90 µm wide, and 65 µm high ridges placed rather close to each other, see Figs. 1e and f. The patterns present differences in both asperity density and contact lengths as well as different possibilities to transport fibers out of the contact.

For comparison, a piece of a conventional grinding stone was obtained from a Swedish pulp mill and cut into a 5 × 5 mm^2 piece, see Figs. 1g and h.

All wood specimens used came from a 50-year-old Norway spruce grown in the middle of Sweden. The wood was preserved by storing it in a freezer directly after cutting. Prior to testing, the wood specimen was placed in the test chamber and heated in a steam atmosphere to reach the desired temperature, taking about an hour. Different tests were performed in sequence along the length of a specimen, avoiding knots and other defects in the wood. After completing the last test on a wood specimen, it was left to dry in a lab environment, *i.e.*, 20 °C and 50% RH.

Table 1. Test Parameters Used in the Grinding Tests

Normal force	10 N
Temperature	70, 90 or 110 °C
Rotational speed	60 RPM
Workpiece diameter	85 mm
Test time	120 s
Repetitions	5

Analysis

The removed amount of fibers was too small to rely on fiber collection and weight measurements for its quantification. Instead, an image-based analysis of the cross section of the grinding tracks was employed to quantify the amount of fibers removed and allow for comparisons between the tests.

When the wood had dried, a 5 mm long section of each grinding track was cut at the position of the circumference where the annual rings were perpendicular to the specimen surface. All analysis was then performed on these sections.

Computed tomography (µCT) was used to measure the area of removed fibers from the cross section of the tracks. It was performed using a Skyscan 1172 (Bruker microCT, Kontich, Belgium) run at 53 kV source voltage and 188 µA source current. The acquired radiographs had a resolution of 1.97 × 1.97 $µm^2$/pixel. From these, the removed area was measured in 50 reconstructed cross sections, spanning a total of 2 mm along each grinding track.

The produced fiber volumes were small, making measurements of conventional pulp properties, such as freeness, impossible. Instead, micrographs of the grinding track's surface and of the released fibers were captured using a Zeiss Leo 1550 scanning electron microscope (SEM; Jena, Germany) to investigate the mechanisms of fiber separation and

the characteristics of the separated fibers. Prior to the SEM imaging, wood and fiber samples were coated with a thin gold/palladium film to reduce surface charging in the microscope.

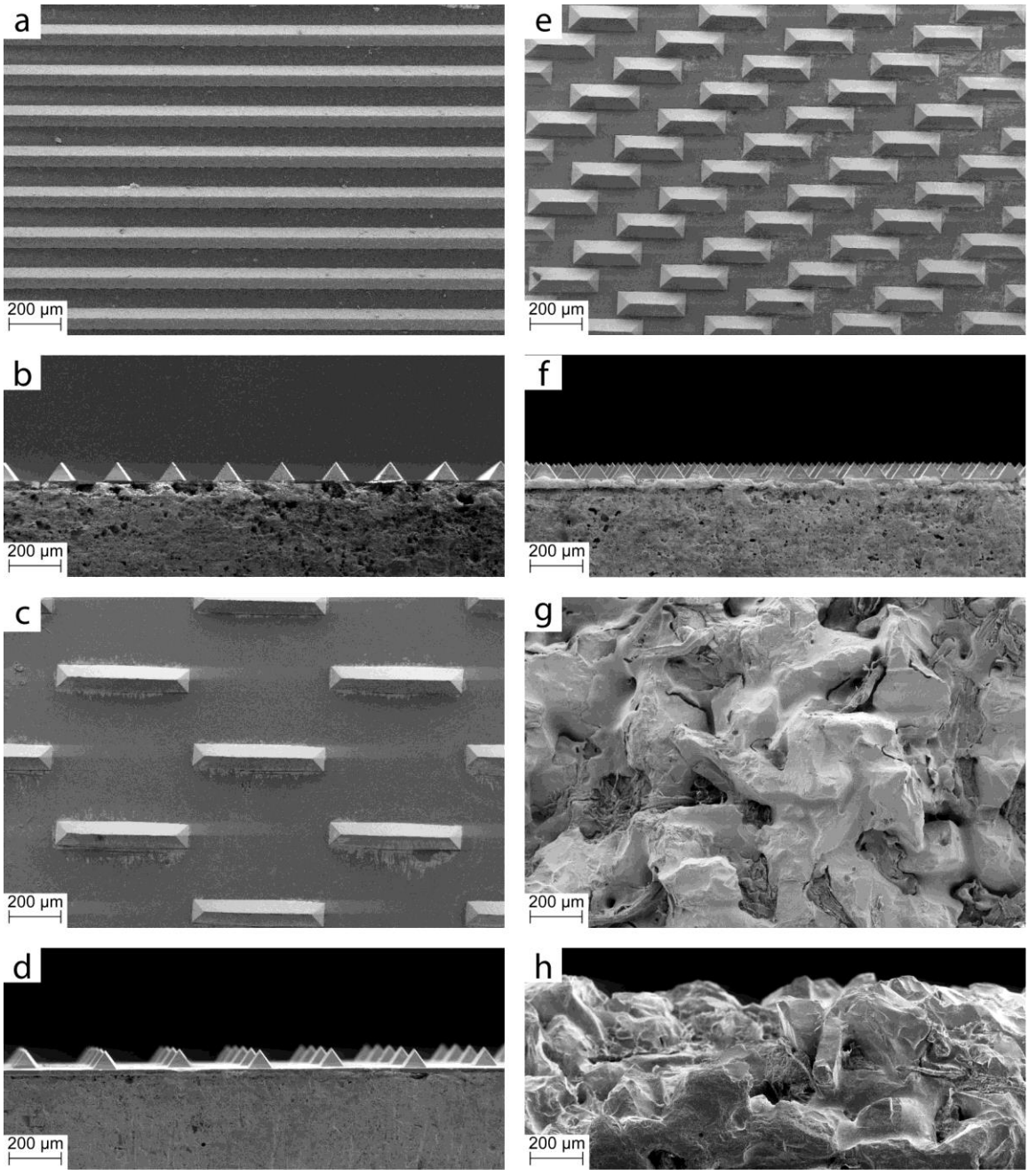

Fig. 1. Parts of the well-defined grinding surfaces; (a-b) long ridges across the whole tool, (c-d) ridges sparsely placed, and (e-f) densely placed. Panels (a), (c), and (e) show the tool from a top view and (c), (d), and (f) show the corresponding tools in cross section. The tool asperities all have a triangular cross section and an apex angle of about 70°. A small piece of a conventional grinding stone with grits about 200 µm in diameter, depicted in (g) top view and (h) in cross section

Grinding Tool Surface Profiles

The four tools present different surfaces to the wood. To be able to relate the grinding tool performance to the surface structure, load bearing curves were produced for all four tools. For the diamond tools, the geometries of the ridges were measured from SEM images, and from these, the load bearing curves were calculated.

The grinding stone surface was analyzed using a ZYGO Nexview NX2 Optical profiler (Middlefield, CT, USA), stitching several images obtained using a 10x magnification lens. Due to poor reflectivity in some areas, the final analysis was made on a 4 × 4 mm^2 area of the grinding stone surface, and a load bearing curve was calculated using the ZYGO Mx software.

Grinding Energy Calculations

The specific grinding energy during each test were calculated from the tangential force and removed fiber cross-section areas, with details presented in a previous work (Heldin and Wiklund 2019). Equation 1 was used to calculate the mass specific grinding energy, E_m,

$$E_m = F_T \omega r t / 2\pi r A \rho = F_T \omega t / 2\pi A \rho \quad (1)$$

where F_T, is the tangential force, ω is the angular velocity, r the radius of the workpiece, t the test time, A the cross-section area of removed fibers, and ρ the density of the wood.

As the angular velocity in the test is 2π rad/s and the test time is 120 s, one can simplify the equation as follows:

$$E_m = 120 F_T / A \rho \quad (2)$$

Assuming a wood density of 400 kg/m^3, the specific grinding energy was calculated using the average measured tangential force and average track cross-section area in each test.

RESULTS AND DISCUSSION

The tangential force showed a changing behavior in the beginning of most tests, lasting some tens of seconds, especially at the lowest temperature (Fig. 2), similar to a running-in behavior of sliding mating surfaces. After this, the tangential force generally stabilized.

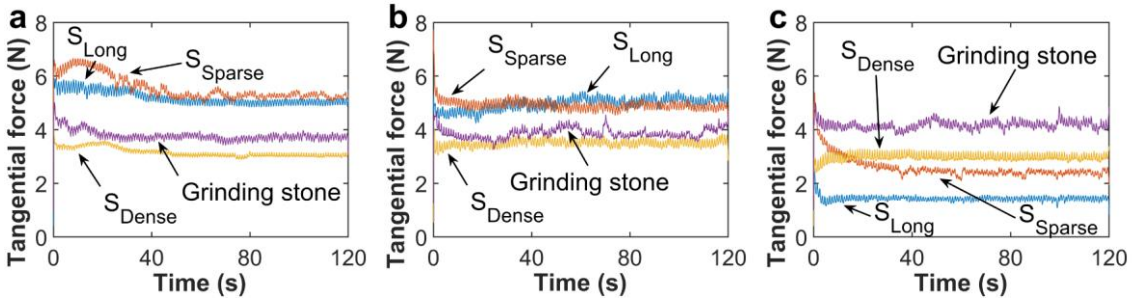

Fig. 2. Representative examples of tangential forces from tests run at (a) 70 °C, (b) 90 °C, and (c) 110 °C

The average tangential force varied between tests for any specific tool and temperature (Fig. 3), but on average all four grinding tools showed reduced average tangential force with increased temperature, especially when going from 90 to 110 °C. The degree of reduction was different for each tool, with S_{Long} showing the largest reduction in tangential force, and S_{Dense} and the grinding stone showing only a slight reduction.

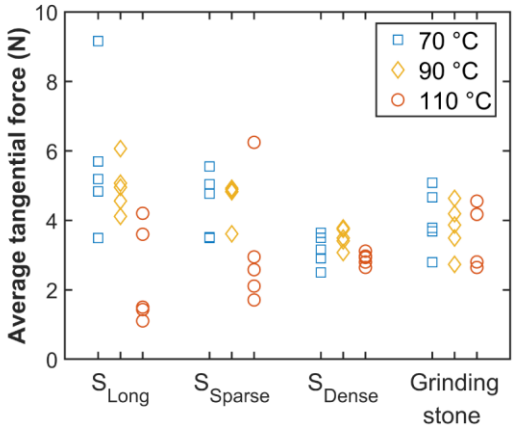

Fig. 3. Average tangential forces for all 60 tests performed

The µCT cross section images in Figs. 4 and 5 show that S_{Long}, S_{Dense}, and the grinding stone show similar trends with increasing areas of fiber removal as the temperature increased.

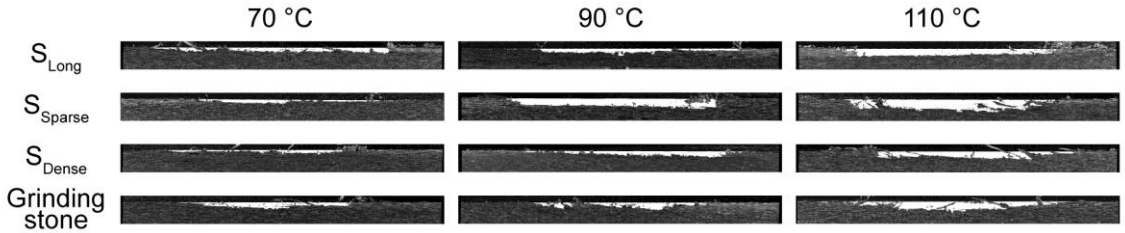

Fig. 4. Examples cross section images obtained using µCT. The grinding tools have moved perpendicular to the image plane and the areas of removed fibers have been highlighted. All images have the same magnification and the tracks are all 5 mm wide.

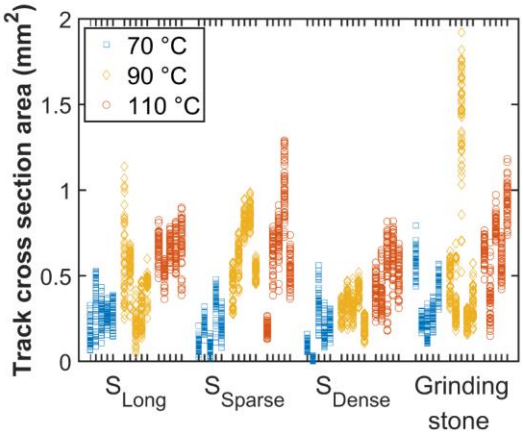

Fig. 5. Measured area of removed fibers from the µCT cross section images, with a total of 50 measurements for each sample

S_{Sparse} showed a large increase in area as the temperature increased from 70 to 90 °C, but then not much larger when increasing the temperature to 110 °C.

The calculated specific grinding energies for the tests (Fig. 6) showed some scatter between the individual tests performed with a specific tool. The spread was large at 70 °C, but much smaller at higher temperatures. For every tool, however, the trend was similar in that the specific grinding energy was reduced as the temperature increased. The lowest specific grinding energy was measured during grinding with S_{Long} at 110 °C, followed by S_{Sparse} at 110°C.

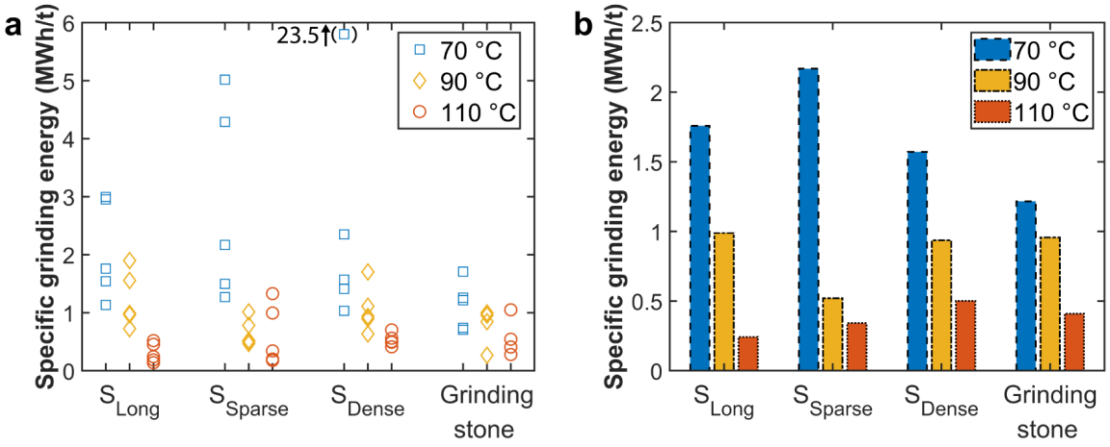

Fig. 6. The specific grinding energy for each of the 60 tests (a) and the median specific grinding energy for the different surfaces at three different temperatures (b)

SEM micrographs of the grinding tracks (Fig. 7) look decievingly similar at first sight, but there are differences. Generally, for all grinding tools the length of the partly separated fibers, *i.e.*, of those still attached to the wood, increased with increasing temperature. S_{Long} and the grinding stone both showed long partly separated fibers at all temperatures. At the lower temperatures, however, the grinding stone tended to cut the fibers, visible in the micrograph from the 70 °C tests in Fig. 7. Additionally, S_{Sparse} and S_{Dense} left grinding tracks with many similarities. When grinding at 70 and 90 °C, both surfaces generally had a low amount of partly separated fibers, and those present were short and fractured.

Images of the released fibers, shown in Fig. 8, reveal that at the lower temperatures all tools produced short fibers together with fragments and fines. The fines tended to gather into bundles or rolls, especially the fines produced at 70 °C. For all four tools, the length of the fibers increased with increasing temperature. For the diamond surfaces, a change in fiber character was found only at 110 °C, whereas for the grinding stone there was a gradual change when going from 70, to 90, and 110 °C. At 110 °C all tools produced long fibers with a lower amount of small fragments and fines. The least damaged fibers were obtained with S_{Sparse}.

The load bearing curves, see Fig. 9a, show that the grinding stone has a much deeper surface profile than any of the diamond surfaces. In Fig. 9b, rescaled to visualize the differences between the diamond surfaces, the surface profiles of S_{Long} and S_{Dense} are very similar and clearly different from S_{Sparse}. These differences are further illustrated in Fig. 10, showing that at identical load bearing areas, here shown as 15%, the shape and distribution of the areas carrying the load are very different for the respective tools.

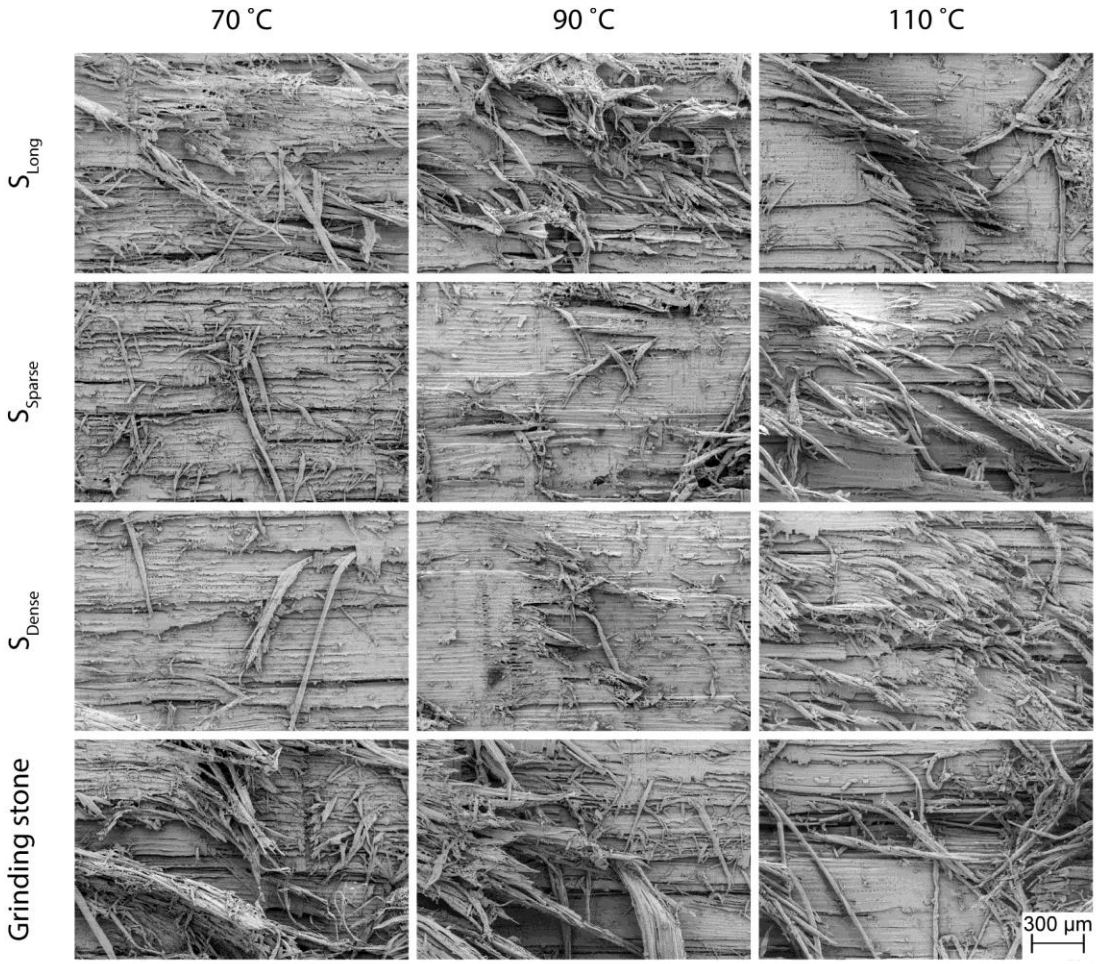

Fig. 7. Representative SEM micrographs of grinding track surfaces for each tool at the three temperatures

Discussion

Obviously, the lateral forces varied somewhat between tests performed with the same test conditions. However, a certain variation is to be expected, as wood is not an isotropic material and has natural variations.

The average tangential force decreased with increasing temperature for all grinding surfaces. This is mostly due to the thermal softening of the wood, which has several effects on the grinding process. The tangential force can be seen as a combination of adhesive and ploughing (deforming) contributions. The ploughing component is directly controlled by the penetration depth of the asperities, which in turn is controlled by the load bearing curve of the surface, illustrated in Fig. 9. When the wood softens, the area over which the load is distributed increases, and the penetration of the asperities into the wood increases. Having different bearing curves, the tool surfaces behave slightly different in this respect, but all of them respond by pushing their asperities deeper as the wood softens. If this was the only effect of the wood softening, then the tangential force would increase. However, as the tangential force is in fact reduced, the softening must also lower the force needed to move an asperity through the wood.

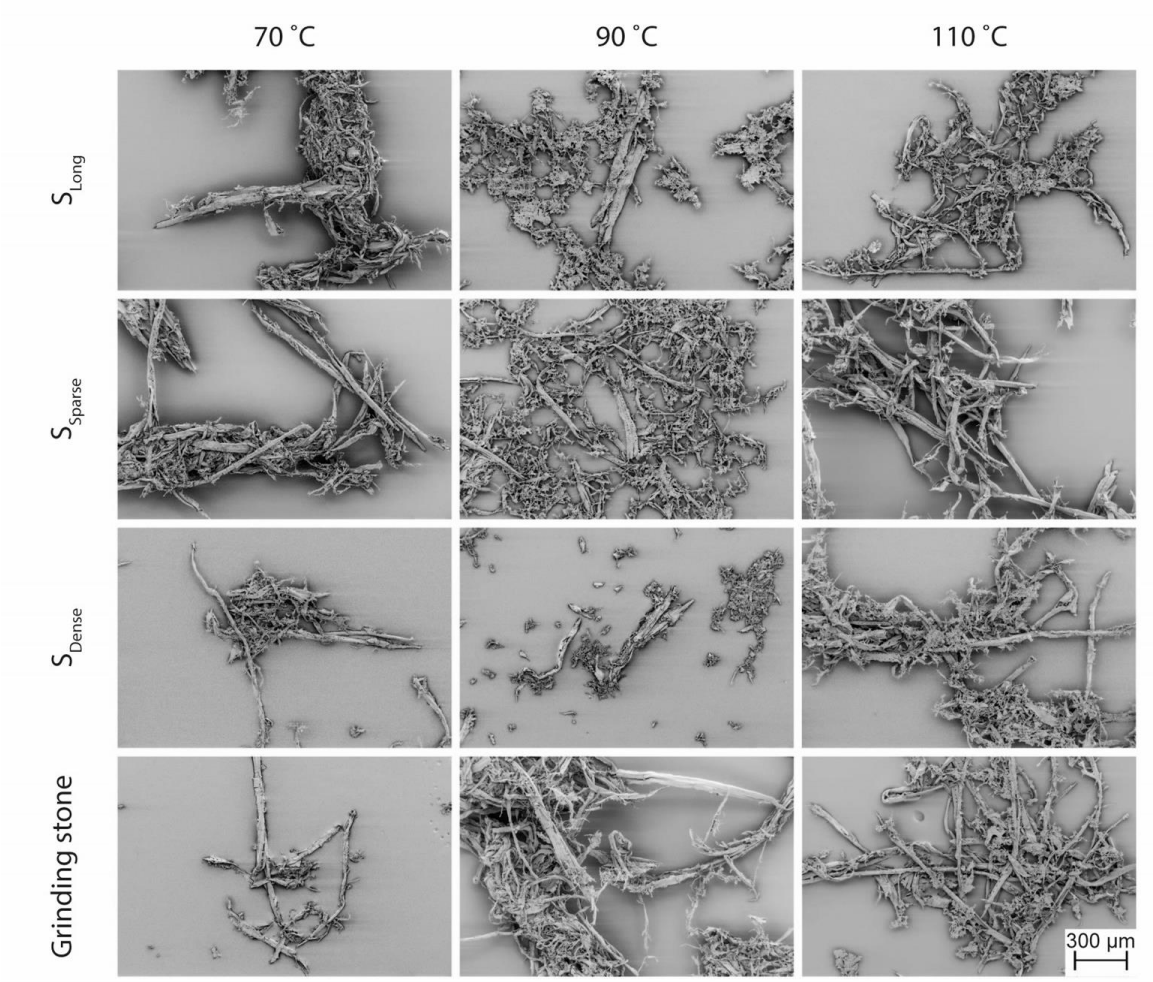

Fig. 8. Representative SEM micrographs of the produced fibers for each tool at the three temperatures

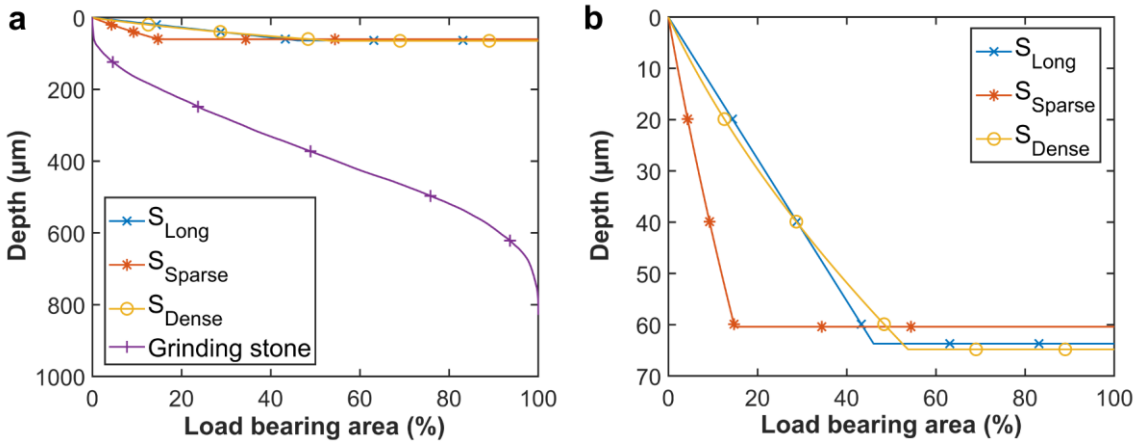

Fig. 9. Load bearing curves for the grinding tools, with (a) all four tools and (b) only the three diamond tools

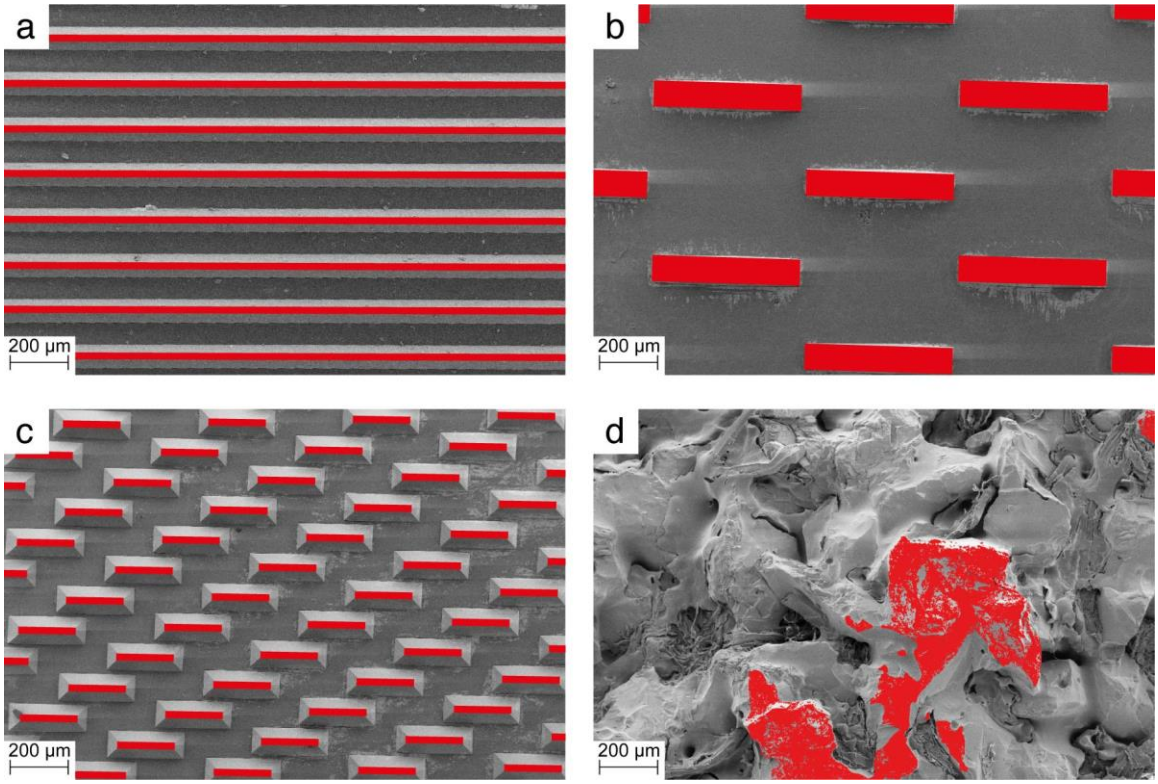

Fig. 10. Illustration of the load distribution over the surfaces at 15% load bearing area, (a) S_{Long}, (b) S_{Sparse}, (c) S_{Dense}, and (d) the grinding stone

The softening makes deforming the cell structure easier. Moreover, lignin is one of the constituents of wood that is affected by an increase in temperature. As the middle lamella between the fibers mostly consists of lignin, the force needed to separate the fibers is lowered drastically. These effects greatly influence the shearing motion and the fiber release, where tensile and shear forces are needed. These effects are larger and more important, it appears, than the effect the softening has in allowing the asperities to penetrate deeper.

Interestingly, the area of removed fibers for S_{Sparse} did not increase as the temperature was increased from 90 °C to 110 °C. It should be noted that S_{Sparse} is the diamond tool that would first allow the wood to contact the flat surface in between the asperities as penetration is increased. Figure 10 shows the situation where S_{Sparse} is on the verge of needing the flat surface to support the load, while the two other diamond surfaces allow even higher load bearing area with only the ridge sides. This can have two effects, which would both hinder the asperities' ability to penetrate further into the wood, despite further softening as the temperature is raised from 90 to 110 °C. Either the wood is indeed contacting the flat surface already at 90 °C or the gap between the flat surface and the wood is small and mostly filled with released fibers. Either way, this could mean this tool has reached its highest possible rate of defibration already at 90 °C. The same thing, which can be alleviated by using tools with higher ridges, could of course also plague the other two diamond surfaces, but S_{Sparse} suffered first. It should also be noted that at 110 °C, both S_{Long} and S_{Sparse} had the same level of removal rate as the grinding stone, and S_{Sparse} actually reached that level already at 90 °C. This is an alternative way of

realizing lower energy consumption for a fixed defibration rate, lowering the requirements for heating.

For all the different grinding surfaces the specific grinding energy was reduced with increasing temperature as a result of the reduction in tangential force and increase in removed fibers as discussed above. Even though the amount of released fibers did not steadily increase with S_{Sparse}, the reduction in tangential force reduced the specific grinding energy. At 110 °C, S_{Long} achieved the lowest median grinding energy, reducing the energy requirements by several tens of percent compared to the grinding stone. S_{Sparse} also showed lower grinding energy than the grinding stone, but not to the same extent as S_{Long}.

Based on the findings from the analysis of the grinding tracks, it was expected that S_{Long} would produce fibers similar to those produced with the grinding stone at low temperatures. But the grinding stone produced long, although fractured, fibers together with some fines, whereas S_{Long} almost exclusively produced smaller fragments.

The characteristics of the released fibers are likely related to the deformation behavior of the wood and strains the fibers are subjected to. As the grinding stone will have the deepest penetration at any temperature, given the size and distribution of the asperities, it will also have the highest local strains around the asperities. However, this is a double-edged sword, while a deeper penetration promotes fiber separation at low temperatures, the local strain might occasionally become too high and cause cutting and fracturing of the fibers. This leads to a mixture of cut fibers and fragments. Extreme forms of this have been demonstrated previously, using well-defined tools with sharp, four-sided pyramids rather than the ridges used in this work (Carlsson *et al.* 2019). S_{Long} and S_{Dense} are at the other extreme. Unable to penetrate properly into the wood at low temperature they cause very superficial strains, which fragments the fibers instead of separating them. S_{Sparse}, having a sparser distribution of asperities, is in between these two extremes. It penetrates deeper into the wood than the other diamond surfaces and thus has a better capacity to separate the fibers. The length of the released fibers using S_{Dense} and S_{Sparse} at 70 and 90 °C is comparable to the length of the asperity ridges, indicating that the edges of the asperities tend to cut the fibers. At 110 °C this is not the case, suggesting that the flexibility of the fibers is increased, which reduces the risk of undesired cutting.

The character of the produced fibers and fines can also be related to the possibilities for the fibers to move out of the contact zone. In order for fibers separated by S_{Long} to move out of the contact zone, they must be transported over the ridges, which likely cause further damage to the fibers. S_{Dense} has angled channels that could aid in fiber transportation, but they are narrow and, based on the fiber character at 110 °C in Fig. 8, it performed no better than S_{Long}. S_{Sparse} has much more space between the ridges, increasing the possibilities for fiber transport which would let the fibers leave the grinding zone relatively undamaged. The grinding stone provides the largest channels for transport, but although the fibers can leave the grinding zone easily after separation the surface does not produce the same undamaged fibers as S_{Sparse} does.

Apparently, the surface topography influences the grinding process greatly, and the well-defined diamond tool surfaces show great potential to reduce the specific grinding energy when compared with a conventional grinding stone. The grinding stone performed better than the diamond surfaces at the lower temperatures. At 110 °C, the diamond surfaces produced similar or better, *i.e.*, less damaged, fibers using less energy than the stone. Moreover, the tool surfaces used in this work are only a few of the options that could be investigated to determine their influence on asperity geometry. The tool

surfaces can certainly be optimized further in the future and tailored to produce fibers of a specific character.

CONCLUSIONS

1. The well-defined grinding surfaces showed great potential in producing long and less damaged fibers at 110 °C than a grinding stone, and at a substantially lower specific grinding energy.
2. The diamond tools only excelled at high temperature. At 70 °C the grinding stone produced longer fibers than the diamond tools did, as the latter could not penetrate sufficiently into the wood to achieve efficient defibration.
3. The influences of temperature on the fiber characteristics and energy consumption were larger for the well-defined diamond grinding surfaces than for the grinding stone.
4. The distribution and density of asperities on the tool surface affect the possibilities for the released fibers to move out of the contact zone. During such transport, a surface with densely placed asperities can damage the fibers more than a surface with sparsely placed asperities.

ACKNOWLEDGMENTS

The Swedish Energy Agency is gratefully acknowledged for financing this study through grant 37206-2.

REFERENCES CITED

Björkqvist, T., and Lucander, M. (2001). "Grinding surface with an energy-efficient profile," in: *Proc. Int. Mech. Pulp. Conf. 2001*, Helsinki, Finland, pp. 373-380.

Björkqvist, T., Tienari, M., and Lucander, M. (2007). "Simulation of fatigue related variables in wood grinding," in: *Proc. Int. Mech. Pulp. Conf. 2007*, Minneapolis, MN, USA, pp. 1-21.

Blechschmidt, J., Engert, P., and Stephan, M. (1986). "The glass transition of wood from the viewpoint of mechanical pulping," *Wood Sci. Technol.* 20, 263-272. DOI: 10.1007/BF00350984

Carlsson, J., Heldin, M., Isaksson, P., and Wiklund, U (2019). "Investigating tool engagement in groundwood pulping – Finite element modelling and in-situ observations at the microscale," Accepted for publication in *Holzforschung*, September 2019.

Campbell, W. B. (1934). "Groundwood studies; theoretical efficiency," *Pulp Pap. Canada* 35, 218-219.

Enström, E., Fagerhed, J. A., and Lönnberg, B. (1990). "Effect of pulpstone grits in wood grinding. Part 1. Distribution of single-size grits," *Pap. Puu* 72(4), 385-390.

Gåhlin, R., Björkman, H., Rangsten, P., and Jacobson, S. (1999). "Designed abrasive diamond surfaces," *Wear* 233-235, 387-394. DOI: 10.1016/S0043-1648(99)00219-7

Heldin, M. and Wiklund, U. (2019). "Defibration mechanisms and energy consumption in the grinding zone – a lab scale equipment and method to evaluate groundwood pulping tools," Accepted for publication in *Nordic Pulp and Paper Research Journal*, October 2019.

Koran, Z. (1981). "Energy consumption in mechanical fibre separation as a function of temperature," *Pulp Pap. Canada* 82(6), 40-44.

Lönnberg, B., Finell, M., and Gros, G. (1996). "Basic study of pulpstone dullness," *Pulp Pap. Canada* 97(10), 341-344.

Nurminen, I., Saharinen, E., and Sirviö, J. (2018). "New technology for producing fibrillar fines directly from wood," *BioResources* 13(3), 5032-5041. DOI: 10.15376/biores.13.3.5032-5041

Pettersson, U., and Jacobson, S. (2006). "Tribological texturing of steel surfaces with a novel diamond embossing tool technique," *Trib. Int.* 39(7), 695-700. DOI: 10.1016/j.triboint.2005.06.004

Salmi, A., Salminen, L. I., Lucander, M., and Haeggström, E. (2012a). "Significance of fatigue for mechanical defibration," *Cellulose* 19, 575-579. DOI: 10.1007/s10570-011-9640-x

Salmi, A., Montonen, R., Salminen, L. I., Suuronen, J. P., Serimaa, R., and Hæggström, E. (2012b). "Cyclic impulsive compression loading along the radial and tangential wood directions causes localized fatigue," *J. Appl. Phys.* 112(12), 124913. DOI: 10.1063/1.4771929

Sandås, E. (1991a). "Effect of pulpstone grits in wood grinding. Part 3. Two-size grit mixture (various sizes)," *Pap. Puu* 73(7), 641-650.

Sandås, E. (1991b). "Effect of pulpstone grits in wood grinding. Part 4. Concluding discussion," *Pap. Puu* 73(9), 858-864.

Sandås, E., and Lönnberg, B. (1990). "Effect of pulpstone grits in wood grinding. Part 2. Two-size grit mixture (various proportions)," *Pap. Puu* 72(8), 765-771.

Tuovinen, O., and Fardim, P. (2015). "Interrelation between grit morphology and defibration performance in pressurized groundwood process," *O Papel* 76(10), 83-89.

Tuovinen, O., Fardim, P., and Lönnberg, B. (2008). "An investigation into topographic changes in pulpstone grits and their impact on pulp quality during the stabilization process," *Pap. Puu* 90(7), 38-43.

Tuovinen, O., Fardim, P., and Wiinamäki, A. (2009). "Initial fiber effects in pressurized grinding as analyzed by SEM," *Proc. Int. Mech. Pulp. Conf. 2009*, Sundsvall, Sweden, pp. 111-116.

Uhmeier, A., and Salmén, L. (1996). "Repeated large radial compression of heated spruce," *Nord. Pulp Pap. Res. J.* 11(3), 171-176. DOI: 10.3183/npprj-1996-11-03-p171-176

Article submitted: May 13, 2019; Peer review completed: October 1, 2019; Revised version received and accepted: October 9, 2019; Published: October 21, 2019.
DOI: 10.15376/biores.14.4.9575-9587